Absolute triple differential cross section for ionization of helium near threshold

T. Rösel, J. Röder, L. Frost, K. Jung, and H. Ehrhardt
Fachbereich Physik, Universität Kaiserslautern, D-6750 Kaiserslautern, Germany

S. Jones and D. H. Madison
Laboratory for Atomic and Molecular Collisions, University of Missouri–Rolla, Rolla, Missouri 65401
(Received 21 April 1992)

Absolute measurements with an accuracy of 22% and theoretical results in a distorted-wave Born approximation (DWBA) are reported for the triple-differential cross section for 26.6-eV electron-impact ionization of helium. An apparatus is used that allows all scattering angles to be independently varied for both coplanar and noncoplanar geometries. The measurements are compared with a DWBA calculation that includes exchange distortion in the calculation of the distorted waves, as well as with earlier calculations by Crothers [J. Phys. B **19**, 463 (1986)] and Pan and Starace [Phys. Rev. Lett. **67**, 185 (1991)]. Emphasis is placed on understanding the mechanisms for near-threshold ionization.

PACS number(s): 34.80.Dp

I. INTRODUCTION

The most detailed information about the electron-impact ionization of atoms is available from $(e,2e)$ electron-coincidence spectroscopy, in which both the final-state electrons following an ionizing event are detected in coincidence. The experiment determines the incident energy E_0, the final-state electron energies E_1 and E_2, and the momenta $\mathbf{k}_1$ and $\mathbf{k}_2$ of the electrons (for a more detailed description, see, e.g., Ehrhardt *et al.* [1] or Lahmam-Bennani [2]). As a result, the kinematics of each ionizing event is fully determined, thus providing a measurement of the triple-differential cross section (TDCS).

The experimental variables and geometries are defined in Fig. 1. For the case of equal outgoing-electron kinetic energies, the angle Θ_{12} between the two outgoing electrons, together with the polar angles ϑ_1 and ϑ_2, fully define the kinematics of the ionizing collision. It is sometimes convenient to refer to the azimuthal angle φ_2 (where φ_1 is defined to be zero), and also to the angle $\chi_{12}=\vartheta_2-\vartheta_1$. In this work the incident-electron energy E_0 is set to 26.6 eV, i.e., 2 eV above the threshold for ionization of helium.

The goal of the present work is to advance the understanding of ionization near threshold by presenting extensive absolute TDCS measurements and theoretical calculations for helium in a set of kinematics designed to test different aspects of the reaction. A comparison with absolute measurements yields a severe test of theoretical models and in some cases permits the isolation of important physical effects in the reaction.

The distorted-wave Born-approximation (DWBA) model presented here includes exchange of continuum and target electrons in the formation of the distorting potentials and is an improvement over the previously reported model of Jones, Madison, and Srivastava [3]. Two other theoretical approaches are also discussed: Crothers [4] has obtained an approximate semiclassical solution of the Schrödinger equation for singlet scattering and Pan and Starace [5] have performed a DWBA calculation for $\Theta_{12}=180°$ where the effects of exchange are included in a nonlocal distorting potential.

Full details of the apparatus and method of measuring absolute TDCS have been reported in Rösel *et al.* [6] and will not be repeated here. The method is based upon measurements of beam-target overlap densities using known absolute total ionization cross sections and of electron-detection efficiencies using known absolute double-differential cross sections. The quoted standard deviation of 22% is derived by Rösel *et al.* from the standard deviation due to counting statistics (3%), due to various measurement tolerances (8%), and due to the precision of the absolute total ionization cross section (10%).

Previous measurements have been restricted to some particular geometry, which, together with the choice of particular electron energies, reduces the number of variables and acts as a "filter" to select certain types of ionizing events. A number of different geometries (kinematics) are shown schematically in Fig. 1. Each emphasizes particular physical effects. All of these kinematics are now accessible in the experiment reported here and will be discussed.

The outline of this paper is as follows. In Sec. II a brief review of the various kinematics and previous experiments is given. The present DWBA model as well as other theoretical models tenable at low impact energies is then discussed in Sec. III. Section IV contains a comparison of theory and experiment. Emphasis is placed on testing the various theoretical assumptions and on isolating different aspects of the ionization reaction. The conclusions are summarized in Sec. V.

II. REVIEW OF KINEMATICS AND EXPERIMENTS

The schematic representation of electron-impact ionization shown in Fig. 1(a) shows the general polar coordi-

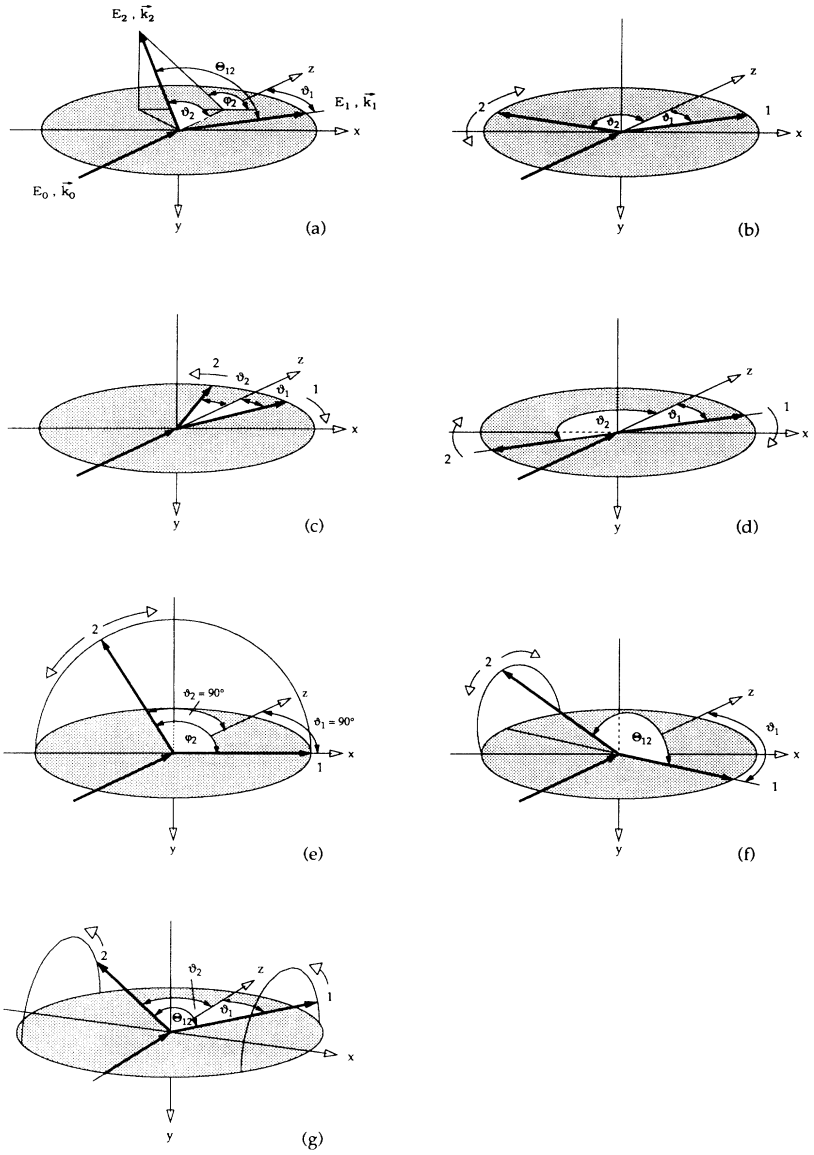

FIG. 1. Electron-impact ionization kinematics: (a) general coordinate system and experimental parameters; (b) coplanar asymmetric kinematics; (c) coplanar symmetric kinematics; (d) coplanar constant mutual angle Θ_{12}; (e) perpendicular plane kinematics; (f) noncoplanar constant mutual angle Θ_{12} for fixed ϑ_1; (g) noncoplanar constant mutual angle Θ_{12} and constant $\chi_{12}=\vartheta_2-\vartheta_1$.

nates for out-of-plane measurements. The thick arrows represent electron trajectories. There are three degrees of freedom in angle (e.g., ϑ_1, ϑ_2, and φ_2) and two in energy (e.g., E_0 and E_1). Four particular combinations of these variables have been used in previous near-threshold experiments: the coplanar asymmetric geometry [Fig. 1(b)], the coplanar symmetric geometry [Fig. 1(c)], the coplanar Θ_{12} geometry [Fig. 1(d)] and the perpendicular plane geometry [Fig. 1(e)]. These geometries and others accessible with the present apparatus will now be defined and briefly discussed.

Coplanar asymmetric ($\varphi_2=0°$ or 180°; ϑ_1 fixed; ϑ_2 varied). Coplanar asymmetric kinematics [Fig. 1(b)] are dominated at higher energies (above about ten times the ionization potential) by scattering of one electron with small energy loss into small angles ϑ_1 [1]. Near threshold, however, the emission probability as a function of the energy of the escaping electron tends to be more nearly constant [7] and the angular distributions are much less forward peaked. Extensive measurements have been made at 1, 2, 4, and 6 eV above threshold by the authors of Ref. [8] and in this group [9,10].

Coplanar symmetric ($\varphi_2=180°$; $E_1=E_2$; $\vartheta_1=\vartheta_2$; ϑ_1, and hence ϑ_2, varied). Coplanar symmetric kinematics [Fig. 1(c)] are governed entirely by singlet scattering. The momentum transfer to the ion core varies over a wide range, from zero to maximum values at large ϑ_1. This has provided a sensitive test, particularly at higher energies, of the projectile-core interaction in theories of ionization that extend beyond first order, e.g., second-order Born and distorted-wave calculations [10,11].

Coplanar constant-Θ_{12} ($\varphi_2=0°$ or 180 °; constant Θ_{12}; ϑ_1, and hence ϑ_2, varied). Constant-Θ_{12} kinematics [Fig. 1(d)] represent the condition under which a simplified

partial-wave analysis of the scattering near threshold is feasible (see below). Furthermore, the postcollision interaction between the two outgoing electrons remains constant. This geometry has been used extensively to investigate Wannier-law angular distributions [12]. The case where both electrons emerge in exactly opposite directions (i.e., $\Theta_{12}=180°$) has received particular attention [13] and is illustrated in Fig. 1(d).

Perpendicular plane ($\vartheta_1=\vartheta_2=90°$; φ_2 varied). Perpendicular plane kinematics [Fig. 1(e)] select those ionizing events where a strong projectile-core interaction has usually occurred. Cvejanovic and Read [14] performed measurements for $\varphi_2=150°$ and 180° in the energy range from 0.2 to 3.0 eV above threshold. Jones *et al.* [15] measured the distribution for φ_2 at 1 and 2 eV above threshold.

Noncoplanar constant-Θ_{12} (constant Θ_{12} and ϑ_1; ϑ_2, and hence φ_2, varied). This geometry [Fig. 1(f)] has become accessible with this apparatus and allows the investigations referred to above to be continued out of plane.

Constant χ_{12} (constant Θ_{12}; ϑ_1, and hence φ_2 and ϑ_2 are varied). This geometry allows several tests of the experimental method and of the reaction theory and is discussed later. The geometry is similar to that shown in Fig. 1(g) (which represents, in fact, the special case $\chi_{12}=\vartheta_2-\vartheta_1=0$).

Noncoplanar symmetric constant-Θ_{12} (constant Θ_{12}; $\vartheta_1=\vartheta_2$; ϑ_1, and hence ϑ_2 and φ_2, varied). This geometry [Fig. 1(g)] further restricts the scattering in the above case to events where only singlet scattering contributes.

III. THEORY

A. Overview

Various effects contribute to, or influence, the calculation of the ionization cross section near threshold: Direct scattering of an electron of momentum $\mathbf{k}_0$ into a state with momentum $\mathbf{k}_1$, with sufficient energy transfer to ionize the target, is described by the amplitude $f(\mathbf{k}_0;\mathbf{k}_1,\mathbf{k}_2)$. Exchange scattering, described by the amplitude $g(\mathbf{k}_0;\mathbf{k}_1,\mathbf{k}_2)$, takes into account the indistinguishability of the two electrons in the outgoing channel, where $g(\mathbf{k}_1,\mathbf{k}_2)=f(\mathbf{k}_2,\mathbf{k}_1)$. The capture process, in which the projectile electron remains with the positive ion core and the two electrons from the target are ejected, is denoted by the amplitude $h(\mathbf{k}_1,\mathbf{k}_2)$. A process known as shakeoff can contribute to both f and g: for shakeoff the incident electron "collides" with the target—either the nucleus or one of the bound electrons—and one of the "untouched" target electrons is ejected.

The cross section is given by

$$\frac{d^3\sigma}{d\Omega_1 d\Omega_2 dE_2}=\frac{(2\pi)^4}{E_0}(|f-g|^2+|f-h|^2+|g-h|^2)\ , \tag{1}$$

where the flux factor results from choosing the continuum wave functions to be normalized to a δ function in energy.

Until recently there were no detailed theoretical calculations of the triple-differential cross section near threshold. Comparison by Schlemmer *et al.* [13] of relative measurements for hydrogen and helium at 4 eV above threshold in the coplanar $\Theta_{12}=180°$ geometry [Fig. 1(d)] showed quite different angular behaviors. The authors argued that, since the final boundary conditions of three charged particles in the continuum are identical, the differences must be due to effects such as atomic polarization, or to the absence of the capture process in the case of hydrogen.

Some simple theoretical models have been investigated. For example, the semiclassical model of Wannier [16], describing the escape of two electrons from a positive ion, was modified by Rau [17] and by Selles *et al.* [12] to include partial waves beyond the ^1S (e.g., $L=1,2,\ldots$).

It is also possible [18] to analyze the scattering in terms of partial waves in a model-independent approach, as follows. Assume first that only the $L=0,1$, and 2 partial waves contribute significantly near threshold. Assume also that the final-state wave function can be written as a two-electron wave function, i.e., in terms of singlet and triplet components. In the present work, where the helium atom and ion are in the ground states, the angular momentum of the incoming and of the two outgoing electrons must be equal and the projections on the electron-beam axis (z axis) are zero. Conservation of parity eliminates states with odd parity. The $^3S^e$ state is suppressed for equal outgoing-electron energies [19]. Thus only the two-electron states $^1S^e$, $^1P^o$, $^3P^o$, $^1D^e$, and $^3D^e$ contribute.

Altick and Rösel [18] have shown that the scattering amplitudes can then be written as functions of the outgoing-electron energy and the mutual angle Θ_{12} between the two final-state electrons, together with geometric factors which depend on ϑ_1 and ϑ_2. The triple-differential cross section σ can then be written using the above five partial waves:

$$\begin{aligned}\sigma&=|f_{^1S}+f_{^1P}+f_{^1D}|^2+|f_{^3P}+f_{^3D}|^2\\&=|F_{^1S}+F_{^1P}e^{i\phi_{^1P}}(\cos\vartheta_1+\cos\vartheta_2)+F_{^1D}e^{i\phi_{^1D}}[P_2(\cos\vartheta_1)+P_2(\cos\vartheta_2)]+F_{^1D'}e^{i\phi_{^1D'}}(3\cos\vartheta_1\cos\vartheta_2-\cos\Theta_{12})|^2\\&\quad+|F_{^3P}(\cos\vartheta_1-\cos\vartheta_2)+F_{^3D}e^{i\phi_{^3D}}[P_2(\cos\vartheta_1)-P_2(\cos\vartheta_2)]|^2\ .\end{aligned} \tag{2}$$

Furthermore, it can be shown that if one defines the angles $\chi_{12}=\vartheta_2-\vartheta_1$ and $\phi_{12}=(\vartheta_2+\vartheta_1)/2$, then for constant χ_{12} and constant Θ_{12} the cross section has the form of a power series with terms $\cos^n(\phi_{12})$, with the highest power equal to twice the highest contributing L wave. This has been used in previous work [18] as a test of the validity of the assumption $L\leq 2$.

A somewhat more stringent assumption, derived from

the Wannier model, that the amplitudes in the above equation are just proportional to $\exp(-2\pi/k_{12})$, where k_{12} is the magnitude of the relative momenta $\mathbf{k}_1-\mathbf{k}_2$ of the two outgoing electrons, allowed Shaw and Altick [20] to estimate the partial-wave amplitudes from the coplanar measurements of Fournier-Lagarde *et al.* [8], taking into account the double-differential absolute-cross-section measurements of Pichou *et al.* [21]. Coplanar measurements alone are not in principle sufficient for such a prediction [22]. These amplitudes were in turn used to predict the out-of-plane cross sections for 1, 2, and 4 eV above threshold. In some cases it was predicted that the cross section should increase as one of the detectors moved out of the scattering plane, e.g., for 2 eV above threshold, $\vartheta_1=60°$ and $\vartheta_2=135°$, and also for $\vartheta_1=120°$ and $\vartheta_2=45°$.

There has recently been rapid progress in *ab initio* quantum-mechanical calculations of triple-differential cross sections near to threshold and an attempt is made to summarize this progress below.

Crothers [4] derives a semiclassical final-state two-electron wave function with regular asymptotic behavior that is a good approximation to the solution of the Schrödinger equation for singlet scattering. This model did not explicitly include for the helium target the possibility of capture or shakeoff processes. Second-order effects were neglected. Nevertheless, rather good agreement with coplanar relative TDCS measurements and absolute total ionization cross sections was obtained in many cases. The theory has recently been extended to include $^3P^o$ triplet scattering [23]. Noncoplanar results are not yet available.

Brauner *et al.* [24] reported calculations for atomic hydrogen in which the final-state wave function has the correct form to satisfy the asymptotic boundary conditions for three charged particles. Near-threshold results for helium are not available. The results for hydrogen agreed with the general shape of the cross section in coplanar asymmetric and coplanar constant-Θ_{12} kinematics. The authors showed that much of the observed structure could be explained in terms of the repulsion between the two electrons, the kinematic effects, and the interference between electron-electron scattering and electron-nucleus scattering. The basic Wannier concept, that ionization near threshold should be dominated by processes in which the two electrons escape at about $\Theta_{12}=180°$ to each other, was reproduced by the theory of Brauner *et al.*, but it was noted that at exactly $\Theta_{12}=180°$ the angular distribution was determined primarily by kinematical effects. That is, all Coulomb waves could be replaced by plane waves without strongly changing the shape of the angular distribution.

Botero and Macek [25] have recently considered an alternative formulation of the perturbation series for the electron-electron T matrix that allows the use of Coulomb wave functions with arbitrary Z_{eff} (i.e., not prescribed by the Rudge-Seaton-Peterkop boundary condition). Using Coulomb waves for incident and outgoing electrons, and multiplying the final-state wave function by a Coulomb factor to account for the electron-electron repulsion, excellent agreement was found with the shape of relative TDCS measurements even below 30 eV. Unfortunately, absolute-cross-section calculations are not available for comparison with the results reported here.

Attempts by Walters, Whelan, and Zhang to extend the region of application of a DWBA, which has been successful in describing coplanar symmetric scattering at 200 eV on helium [11], to energies of a few tens of volts above threshold have been moderately successful in the perpendicular-plane geometry, but not for the coplanar symmetric kinematics [26]. A failure of the model at low energies is perhaps not too surprising: The qualitative success of the model of Brauner, Briggs, and Klar with the correct asymptotic wave function shows that the long-range interaction between the two final-state electrons is important. However, these long-range forces are not included in the calculation of the final-state wave functions in the standard DWBA. While the standard DWBA treats a large part of the electron-atom interaction in the initial state and the electron-ion interaction in the final state to all orders of perturbation theory, the electron-electron interaction in the final state is treated only to first order.

Pan and Starace [5] recently reported a distorted-wave (DW) calculation for $\Theta_{12}=180°$ that was in excellent agreement with the measurements of Schlemmer *et al.* [13]. The work of Pan and Starace represents an improvement over the standard DWBA in terms of the following.

(1) The final-state electron-electron interaction is approximately included in the calculation of the final-state wave function through the use of effective charges chosen to satisfy the Rudge-Seaton-Peterkop relation (see Ref. [27], and references therein).

(2) Electron exchange with the target electrons is explicitly taken into account in the calculation of the distorted waves through the use of a nonlocal distorting potential.

DWBA models often do not take exchange into account in the calculation of the continuum wave functions (i.e., the distorting potentials do not distinguish between identical and nonidentical particles). Exchange can have an important effect in the formation of the wave functions, however. We have labeled this effect "exchange distortion."

Furthermore, Pan and Starace used the prior form of the exact T matrix and used a procedure for generating the distorting potentials that guaranteed orthogonality of the bound and continuum target states. This has the effect of causing shakeoff and capture terms to vanish and also causes the post and prior forms of the T matrix to be identical, providing that the autoionizing amplitudes that appear in the post form are ignored [3].

Jones, Madison, and Srivastava (hereafter referred to as JMS) [3] also recently reported an improvement over the standard DWBA as follows.

(1) The final-state electron-electron interaction is approximately included in the calculation of the final-state wave function through the use of angle-dependent effective charges.

(2) Shakeoff and capture amplitudes are calculated. Normally these amplitudes are forced to vanish using orthogonalization procedures; often they are simply ignored.

The JMS results were in qualitative agreement with relative coplanar measurements, but they could not fully reproduce the large amount of scattering observed perpendicular to the beam direction.

The JMS model differs from the calculation of Pan and Starace in the following aspects.

(1) The JMS model does not include exchange distortion.

(2) A different *Ansatz* is used for the effective charges.

(3) JMS calculate shakeoff and capture amplitudes, while Pan and Starace use a formulation where these amplitudes vanish.

(4) The post form of the T matrix is used by JMS, while Pan and Starace use the prior form of the T matrix.

B. Present theoretical model

In this paper, we report an improvement over the JMS model [3]. The primary difference between this model, hereafter referred to as the JM (Jones-Madison) model, and the JMS model is that the JM model includes exchange distortion. The motivation for including exchange distortion was provided by the work of Pan and Starace [28], which showed that exchange effects are needed to explain the large differences that are observed between hydrogen and helium for scattering perpendicular to the incident-beam direction.

The theory without exchange distortion has been completely described in JMS; therefore only an outline of the JM model will be given here. In addition to extending the JMS model to treat exchange distortion, two simplifying assumptions have been made.

(1) If the atomic states are orthogonal to the distorted waves, the capture and shakeoff terms vanish. These states are normally not orthogonal, however, and JMS evaluated the resulting shakeoff and capture amplitudes. One common method for eliminating these amplitudes is to artificially enforce orthogonality by appropriately modifying the continuum wave functions. The wisdom of this approach may be questioned, however, since the continuum wave function can then be significantly altered for the very important small radii. We found that while the standard distorted waves were not orthogonal to the bound states, the distorted waves modified by the exchange distortion (discussed below) were nearly orthogonal to the bound states. Consequently, the JM model is fairly insensitive to forced orthogonalization so we have employed this technique as a matter of convenience.

(2) The sudden approximation is employed since it further simplifies the details of the calculation. In the sudden approximation it is assumed that the helium atom does not have time to relax immediately following the ionizing collision (i.e., it is assumed that the initial and final bound-state orbitals are equal). The JMS and JM models are not sensitive to this assumption.

With these simplifications, the direct (f) and exchange (g) amplitudes are given in the DWBA by [29]

$$f=\left\langle \chi_1^-(0)\chi_2^-(1)\left|\frac{1}{r_{01}}\right|\psi_{1s}(1)\chi_0^+(0)\right\rangle , \tag{3}$$

$$g=\left\langle \chi_2^-(0)\chi_1^-(1)\left|\frac{1}{r_{01}}\right|\psi_{1s}(1)\chi_0^+(0)\right\rangle . \tag{4}$$

The incident distorted wave, χ_0, is an eigenfunction of the initial-state distorting potential U_0, while χ_1 and χ_2 are final-state distorted waves that are obtained as eigenfunctions of potentials U_1 and U_2. ψ_{1s} is the $1s$ Hartree-Fock orbital for helium [30]. In the work of JMS, the initial-state distorting potential U_0 was the static potential of the neutral atom, which is given in atomic units as

$$U_{\text{atom}}(r_0)=-\frac{2}{r_0}+2\left\langle \psi_{1s}(1)\left|\frac{1}{r_{01}}\right|\psi_{1s}(1)\right\rangle . \tag{5}$$

In the JM model, the effects of exchange are included through the use of the Furness-McCarthy [31] exchange potential:

$$U_0(r_0)=U_{\text{atom}}(r_0)+U_{\text{exc}}(r_0) \tag{6}$$

with

$$U_{\text{exc}}=\tfrac{1}{2}\{(E-V)-[(E-V)^2+8\pi|\psi_{1s}|^2]^{1/2}\} , \tag{7}$$

where $V=U_{\text{atom}}$, and $E=E_0$ for U_0. Although this has previously been used for high energies, the present results indicate that it is also a reasonable approximation even near threshold. In the standard DWBA approach, the Coulomb repulsion between the two final-state electrons is ignored in the calculation of the final-state distorted waves and each of these electron wave functions is obtained as an eigenfunction of the static potential of the ion:

$$U_{\text{ion}}(r_0)=-\frac{2}{r_0}+\left\langle \psi_{1s}(1)\left|\frac{1}{r_{01}}\right|\psi_{1s}(1)\right\rangle . \tag{8}$$

However, in the JM model, as in the JMS model, the final-state distorted waves approximately include the three-body Coulomb interaction through the use of an effective charge *Ansatz*. As discussed by JMS, the asymptotic effective charge for equal-energy final-state particles is given by

$$z_1=z_2=1-\frac{1}{2\sin(\Theta_{12}/2)} . \tag{9}$$

The distorting potentials U_1 and U_2 are then formed by taking a linear combination of U_{atom} and U_{ion}, which yields the proper boundary conditions at zero and infinity:

$$U_1(r)=z_1U_{\text{ion}}(r)+(1-z_1)U_{\text{atom}}(r) , \tag{10}$$

$$U_2(r)=z_2U_{\text{ion}}(r)+(1-z_2)U_{\text{atom}}(r) . \tag{11}$$

In this work, the exchange potential (7) is then added to U_1 and U_2, with $V=U_1$ or U_2 and with $E=E_1$ or E_2, as appropriate.

The difference between the present work and the calculation of Pan and Starace [5] are the following.

(1) For $\Theta_{12}=180°$ (the only case considered by Pan and Starace), our asymptotic effective charge is $\frac{1}{2}$, while Pan and Starace use $\frac{3}{4}$ (discussed below).

(2) Pan and Starace include exchange interactions directly in the calculation of the continuum wave functions, while the JM model uses a local approximation for this effect.

We note that although different *Ansätze* are used for the effective charges, Eqs. (10) and (11) are equivalent to the method used by Pan and Starace for forming distorting potentials.

Finally, we note that for the special case of $\Theta_{12}=180°$ the present choice for asymptotic effective charges ($z_1=z_2=\frac{1}{2}$) gives the correct asymptotic potential energy for each electron, but will not satisfy the Rudge relation [27] explicitly unless one properly accounts for the double counting of the final-state electron-electron interaction. This is due to the fact that the Rudge relation is essentially an energy-balance equation for the total potential energy of the system. To obtain the potential energy of the system from an effective charge *Ansatz* such as (9), it is necessary to subtract any interactions that are counted twice when the individual potential energies are added. Then it is easily seen that (9) also gives the correct total potential energy of the system. Pan and Starace [5], on the other hand, have chosen their effective charges so that one obtains the correct asymptotic classical force on each electron. For $\Theta_{12}=180°$, they use $z_1=z_2=\frac{3}{4}$. This *Ansatz* satisfies the Rudge relation explicitly, but does not give the correct asymptotic potential energy for each electron.

IV. RESULTS AND DISCUSSION

We have performed absolute TDCS measurements for kinematics both in and out of the scattering plane. These measurements provide a stringent test for various theoretical models, and, in this section, comparison between experiment and theory will be made for the JM and JMS models, the DW results of Pan and Starace [5], and the calculation of Crothers [4]. The JM and JMS models were obtained for arbitrary energies and angles. Pan and Starace [5] limited their calculations to coplanar $\Theta_{12}=180°$, and the results of Crothers [4] are available only for a limited range of coplanar kinematics.

Before proceeding to a detailed comparison between theory and experiment, we will first illustrate the spatial distribution of the triple-differential cross section. Figure 2 shows in polar coordinates a spline-curve surface fitted to approximately 200 measured data points for the absolute triple-differential cross section with one detector fixed at $\vartheta_1=90°$ and the other detector varied through all possible angles in space. Note that a small intensity, equal to 4% of the maximum, was also measured for ϑ_2 angles between detector 1 and the z axis (electron beam), but this is omitted from the figure for clarity (see, however, Fig. 5). The thick line at $\vartheta_2=90°$ represents the kinematics for $\vartheta_1=\vartheta_2=90°$; that is, the perpendicular plane geometry referred to in the Introduction and shown in Fig. 1(e). The dashed line represents coplanar measurements. The results for both of these particular geometries will be discussed below.

The maximum in the cross section occurs when the second electron is approximately directly opposite the first (i.e., at $\vartheta_2=90°$ and $\phi_2=180°$) as would be expected from the simple picture of electron-electron correlation in the continuum as originally proposed by Wannier. The shape of the distribution is not cylindrically symmetric, however, which means that it is not just a function of the mutual angle Θ_{12} between the two outgoing electrons.

The above results are represented in the more convenient rectangular coordinates in Fig. 3(a), which can be compared directly with the JM theoretical calculations in Fig. 3(b). From this figure we see that while the JM calculation exhibits the correct shape, the magnitude is somewhat smaller than the absolute measurements. The possible reasons for this discrepancy will be discussed later, after considering results in other kinematics in detail.

The spline-fitted cross-section data presented in Fig. 4(a) for $\vartheta_1=60°$ show a more complex structure. There is a clear "valley" or local minimum in the cross section near $\vartheta_2=120°$, i.e., directly opposite detector 1. This contradicts the intuition based on the simple Wannier model, but can readily be explained in terms of contributions from partial waves higher than $L=0$. This point has been discussed for relative, in-plane measurements by Selles *et al.* [8]. The corresponding JM calculations in Fig. 4(b) show good agreement with the shape, but the structure is less sharp and the magnitude is again somewhat smaller.

Shaw and Altick [20] predicted, on the basis of semiempirical estimates, that the out-of-plane TDCS at 2 eV above threshold should be larger than the coplanar value for $\vartheta_1=60°$ and $\vartheta_2\sim135°$. It is obvious from Fig. 4 that

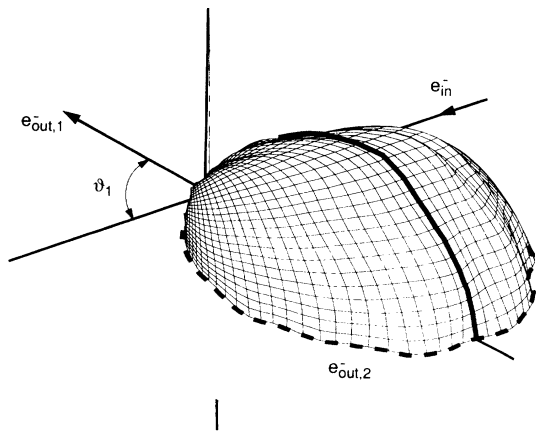

FIG. 2. The measured absolute triple-differential cross section in polar coordinates for $E_1=E_2=1$ eV and ϑ_1 fixed at 90°. The surface is a spline fit to over 200 data points and is marked at 2° intervals. The measurements have a relative uncertainty to each other of 10% and an overall uncertainty in absolute value of 22%. The thick solid line indicates points measured in perpendicular plane kinematics, whereas the thick dashed line indicates coplanar measurements.

this is not correct. The disagreement could be due to the limitations of the data available in the original fitting procedure or to a breakdown in the assumptions in the model.

The first assumption that Shaw and Altick used, that the cross section can be analyzed in terms of the three lowest partial waves, can be tested (as discussed above) by fitting those points with constant Θ_{12} and constant $\chi_{12}=\vartheta_2-\vartheta_1$ with a power series in ϕ_{12}. This test showed that $L=3$ terms were not necessary to describe the results presented here. However, this is only a necessary and not a sufficient condition: Test calculations in the JM model show that although partial waves with $L>3$ contribute only to angular ranges close to the beam direction (i.e., $\vartheta_1,\vartheta_2\rightarrow 0°$ or 180°, which are not experimentally accessible), partial waves with $L=3$ contribute for all angles.

Nevertheless, a number of attempts were made, using several fitting methods [32], to find a set of ten parameters for Eq. (2) which could reproduce our measurements.

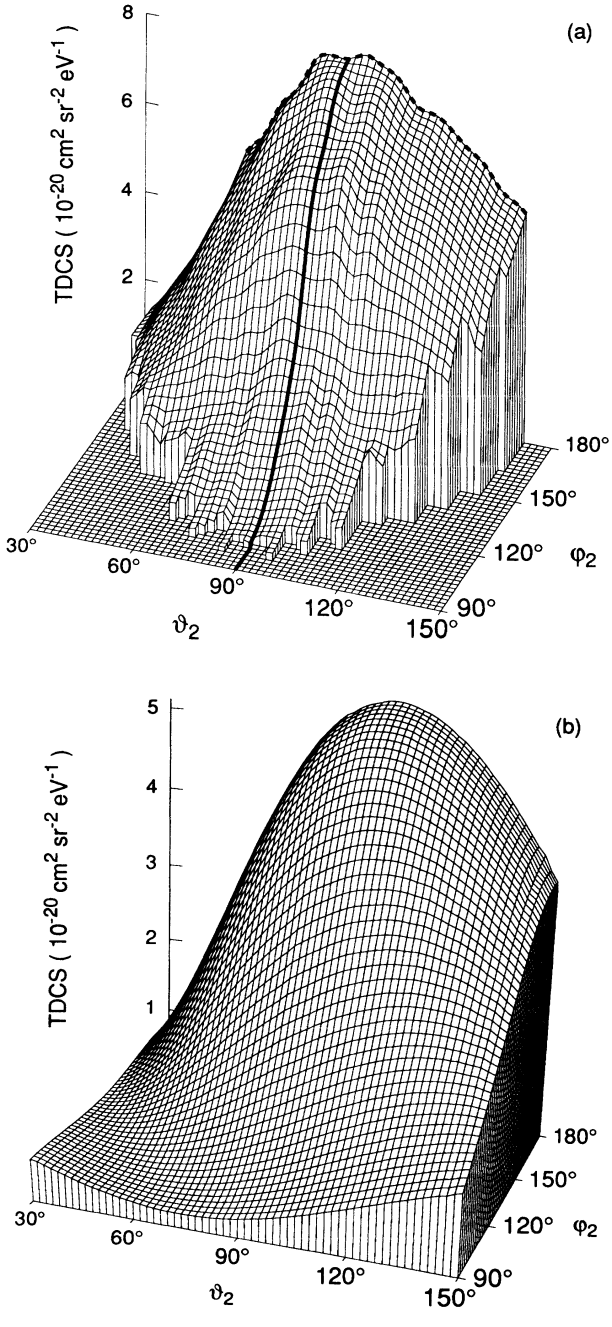

FIG. 3. (a) The measured absolute TDCS as in Fig. 2, but in rectangular coordinates where $\varphi_2=180°$ represents in-plane scattering; (b) the calculated cross section using the JM model corresponding to (a).

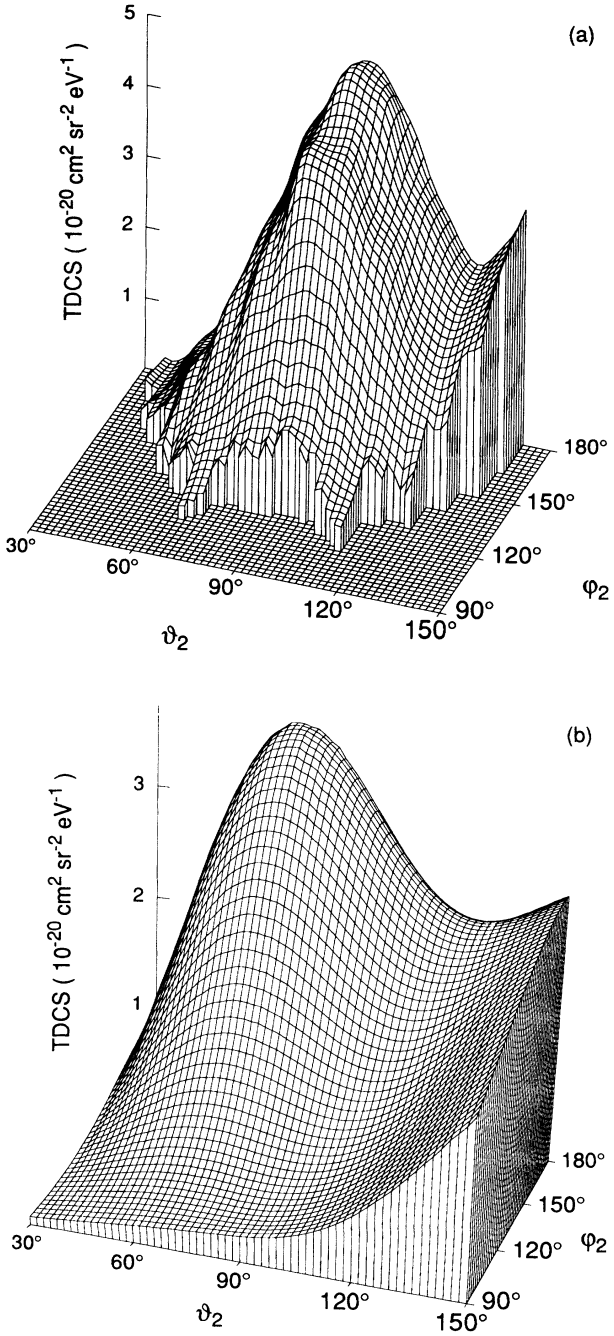

FIG. 4. (a) The measured absolute TDCS, spline-fitted as in Fig. 3, but for ϑ_1 fixed at 60°; (b) the calculated cross section using the JM model corresponding to (a).

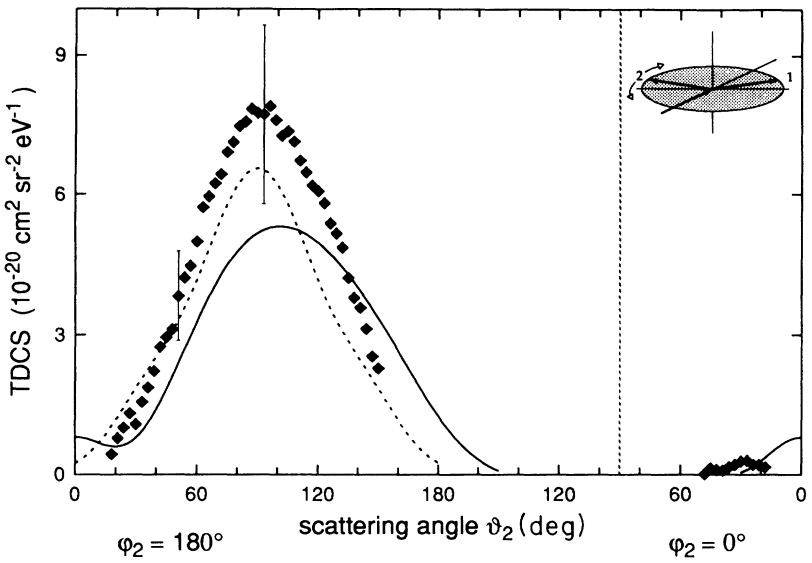

FIG. 5. The measured absolute TDCS for $\vartheta_1 = 90°$ and $\varphi_2 = 0°$ or $\varphi_2 = 180°$. The vertical dashed line indicates the position of detector 1. Detector 2 is rotated within the scattering plane. This corresponds to the measurement fitted by the dashed line in Fig. 2. In this figure, the dotted line shows the theoretical calculation of Crothers [4], the solid line the JM results.

Unfortunately, several equally good and independent solutions were found, showing that the accessible angular range does not permit an unambiguous determination, despite the present extension to out-of-plane kinematics.

The coplanar results from Fig. 3, where ϑ_1 is fixed at 90° and detector 2 is moved in the scattering plane, are shown in detail in Fig. 5, together with calculations from the JM model (solid line) and from Crothers (dotted line). The JM results are in qualitative agreement with experiment, but underestimate the magnitude of the peak and overestimate the shift in the peak position. The small amount of scattering at $\vartheta_2 = 30°$ and $\phi_2 = 0$ (i.e., both detectors on the same side of the electron beam) is predicted by the JM model, but likewise shifted. The theory of Crothers, even though calculated only for singlet scattering, fits the data in these kinematics quite well, although the peak is predicted to be at 90° instead of the actual 100°. Test calculations, within the JM model, show that the main peak is not affected by ignoring the triplet contribution (of course, right at $\vartheta_1 = \vartheta_2 = 90°$ the scattering must be of the pure singlet type). In contrast, the smaller peak results primarily from triplet scattering.

The in-plane results for $\vartheta_1 = 60°$ [Fig. 6(a)] show more clearly the presence of two peaks. Again, results from the JM model and from Crothers are shown for comparison. The JM model shows the double-peak structure, but the location of the first peak is shifted and the overall cross section is underestimated. The first peak, near $\vartheta_1 = 90°$, is predicted rather well by the model of Crothers, indicating that it is still mainly due to singlet scattering. Crothers's results significantly underestimate the second peak, which indicates a strong triplet contribution. Cross-section measurements near 180° are unfortunately not possible due to obstruction by the electron gun. Experimental results are shown for $\vartheta_1 = 120°$ in Fig. 6(b). These show a similar double-peak structure, which is also predicted by the JM model.

To conclude the discussion of coplanar results for fixed ϑ_1, a similar comparison is shown for $\vartheta_1 = 30°$ [Fig. 7(a)] and 150° [Fig. 7(b)]. The JM model is in quite good agreement with experiment in each case. The worsening agreement for the Crothers results is due to increasing contributions to the cross section from triplet scattering.

It is useful here to consider a geometry which has been discussed recently [10,11,33] in terms of direct and double scattering, namely the coplanar symmetric geometry in which ϑ_1 is maintained equal to ϑ_2. The results presented in Fig. 8 are slightly different from those shown

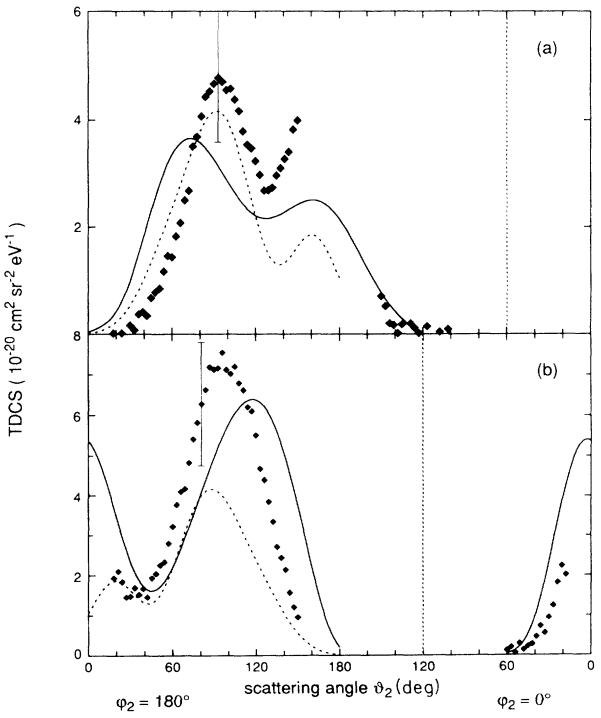

FIG. 6. The measured absolute TDCS for (a) $\vartheta_1 = 60°$, (b) $\vartheta_1 = 120°$. Calculations: Crothers [4], dotted line; JM, solid line.

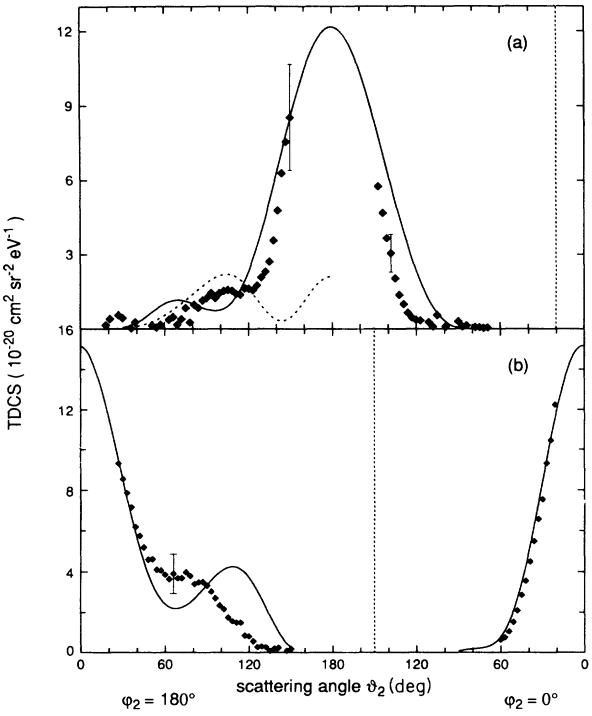

FIG. 7. The measured absolute TDCS for (a) $\vartheta_1=30°$, (b) $\vartheta_1=150°$. The curves are as in the previous figure.

in the near-threshold measurements reported from this laboratory [10]. In these kinematics the apparent position and width of the measured peak depend very sensitively on the alignment and adjustment of the electron beam, and several tests had to be devised to monitor alignment during the course of the measurements. The results in the figure are from a single measurement lasting 2 d, and they are in agreement within statistics with individual measurements made for a range of kinematics (which happened to include some coplanar points with $\vartheta_1=\vartheta_2$) over the course of several months.

As discussed in the Introduction, triplet scattering is suppressed in these symmetric kinematics, so that the Crothers model should be applicable. The measurements show, however, a slight tendency for increased scattering at higher angles, and a breaking of the symmetry about 90°, which was predicted by the model of Crothers. Comparison of theory and experiment at higher energies have shown [10] this effect to be due to second-order terms in the scattering. In particular, it is known that double scattering, in which the incident electron is scattered backwards through a collision with the nucleus before ionizing the target, is important for describing the case in which both electrons emerge in the backward direction. Crothers used a first-order approximation (plane wave) for the incident electron, and so this double collision could not be modeled. The JM model, on the other hand, accounts for double scattering since the projectile-nucleus interaction is included exactly in the formation of the initial-state distorting potential.

The JM model predicts, however, stronger backscattering than is seen in the experiment. We believe that this discrepancy arises primarily from the inability of effective charges to model accurately final states with small electron-electron angular separations. This stems from the fact that an effective charge is "placed" at the origin and thus can only exert a radial force on the outgoing electrons. Thus, effective charges should be more reliable for large angular separations where the Coulomb repulsion between the two final-state electrons is nearly in the radial direction from the residual ion. This conclusion is further supported by the fact that the JM results in Fig. 8 also overestimate the forward scattering when the angular separation is small.

If we demand, for equal energies, that $z_1=z_2$, then the Rudge relation yields the asymptotic effective charge

$$z'=1-\frac{1}{4\sin(\Theta_{12}/2)} . \tag{12}$$

Test calculations showed that using $z_1=z_2=z'$ in the JM model dramatically worsens agreement with experiment,

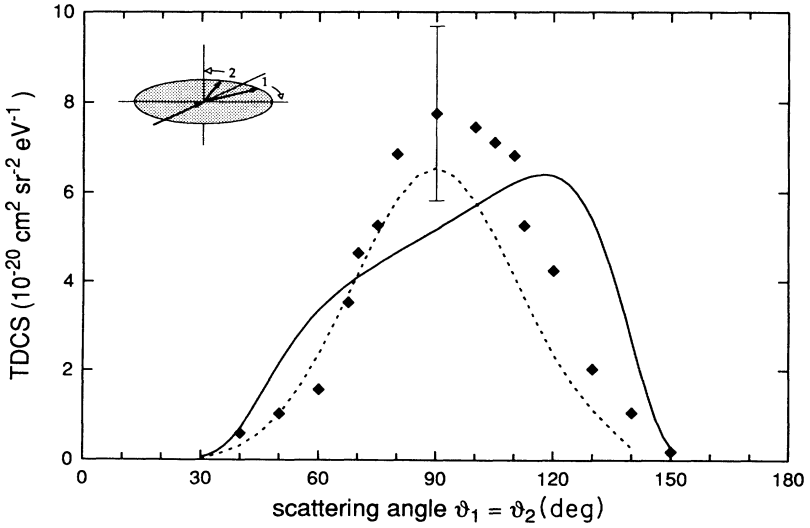

FIG. 8. The measured absolute TDCS for coplanar symmetric kinematics, $\vartheta_1=\vartheta_2$, $\varphi_2=180°$. Theory: JM, solid line; Crothers, dotted line.

causing the single peak for coplanar symmetric geometry to split into two much larger peaks near 50° and 150°, with a pronounced minimum near 90° (where the experimental maximum occurs). Furthermore, we found that using z', rather than (9), worsens agreement for all kinematics in this report (in both the JMS and JM models); the worsening is, however, much more striking for the case of coplanar symmetric scattering.

The above examples show structures resulting from strong electron-electron correlation in the outgoing channel, and in some cases strong distortions in the incident channel. In the case of scattering in the perpendicular plane kinematics [Fig. 1(e)], where $\vartheta_1=\vartheta_2=90°$, and $\vartheta_2=\Theta_{12}$ is varied, structures arising from distortions in the incident channel are expected to be washed out due to the strong Coulomb repulsion at the low energies considered here. This can be seen as follows. With a very simple model, Zhang, Whelan, and Walters [26] were able to show that ionization in the perpendicular plane results from two basic mechanisms. Each of these mechanisms leads, at higher energies, to a peak in the TDCS. First, they considered the possibility of a single collision between the projectile and an atomic electron (no momentum is transferred to the ion) leading to two final-state electrons in the perpendicular plane. Since initially the free momentum in this plane is zero, they argued that two electrons with equal kinetic energies will most likely emerge in opposite directions in the scattering plane. Next, they showed that a simple double collision could be pictured by assuming that the incident electron is first elastically scattered through 90° by the nucleus. This is followed by a collisions with a target electron, which would most likely lead to two electrons emerging 90° apart. Although this double-scattering mechanism is expected to be important near threshold, the strong Coulomb repulsion between the two final-state electrons will dominate and cause these two electrons to emerge with an angular separation greater than 90°. Thus, at sufficiently low energies, only the single peak at $\Theta_{12}=180°$ will remain.

It might be thought that in perpendicular plane kinematics, where only the final-state angular separation is varied, the shape of the angular distribution would depend only on the final-state electron-electron interaction. However, test calculations within the JM model show that this is certainly not the case. In particular, the double-scattering mechanism referred to above increases the relative amount of scattering for angles greater than approximately 90°. Thus perpendicular plane kinematics do not necessarily provide a sensitive test of the *Ansatz* used to model the Coulomb repulsion, since these kinematics cannot isolate the effects of the final-state electron-electron interaction from distortions in the incident channel.

The results shown in Fig. 9, for the perpendicular plane kinematics, are compared here with the JM model. The fact that the JM model underestimates scattering at $\vartheta_1=\vartheta_2=90°$ and $\varphi_2=180°$ has already been demonstrated and discussed. Hence in this figure the JM theory (solid line) has been multiplied by a factor of 1.44 (dashed line) to emphasize the good agreement for the shape of the JM cross sections for final-state angular separations greater than 140°. The effective charge *Ansatz* used here to model the repulsion between the two final-state electrons is expected to break down as the mutual angle Θ_{12} is decreased; the results shown in Fig. 9 suggest that the *Ansatz* works well down to $\Theta_{12}=140°$ for perpendicular plane kinematics.

In contrast to previous kinematics, where electron-electron repulsion was important, Fig. 10 presents results for coplanar kinematics with $\Theta_{12}=180°$ (see inset of Fig. 10), where the repulsion (correlation) between the two outgoing electrons is weakest. Correlations in the target, or distortions in the incident channel, could hence be expected to play a more significant role. Calculations are shown for the models of JM (solid line), JMS (dotted-dashed line), Pan and Starace (dashed line), and Crothers (dotted line).

The recent theoretical treatment by Pan and Starace (dashed curve in Fig. 10) attributes the pronounced peak

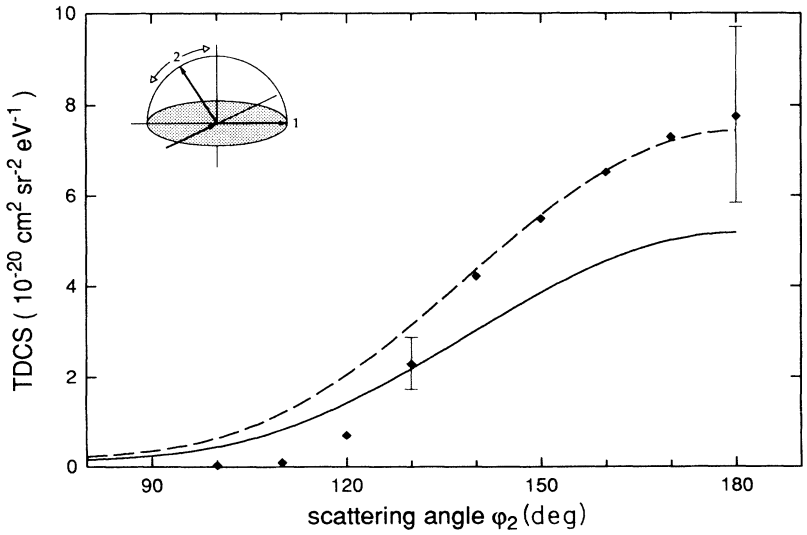

FIG. 9. The measured absolute TDCS for perpendicular plane kinematics, $\vartheta_1=\vartheta_2=90°$, and φ_2 (that is, Θ_{12}) varied. The solid line is the JM result; the dashed line is the JM result, multiplied by 1.44 to allow comparison of relative shape.

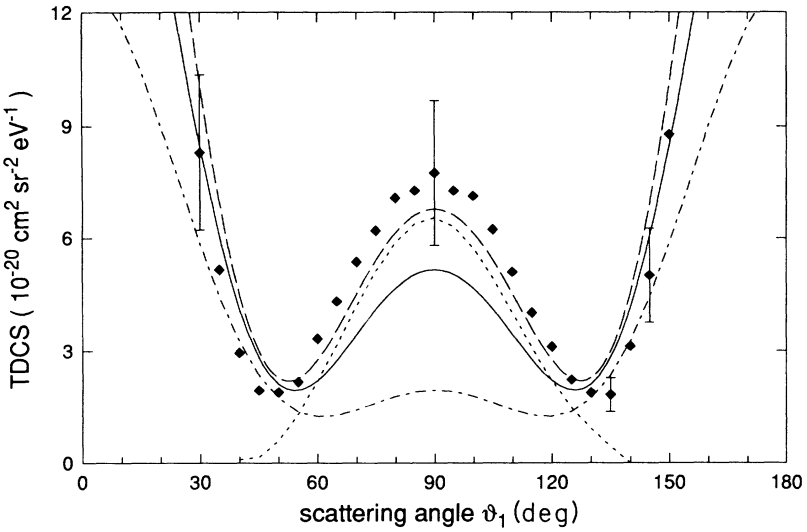

FIG. 10. The measured absolute TDCS for coplanar scattering with $\vartheta_2 = 180° - \vartheta_1$. Theory: JM, solid line; JMS, dashed-dotted line; Crothers, dotted line; Pan and Starace, long-dashed line.

at $\vartheta_1 = 90°$ (where both electrons exit perpendicular to the incident electron beam) to an interference effect between partial waves. In particular, they found that hydrogen and helium were described by similar amplitudes, except that the phase of the amplitude corresponding to a head-on collision (zero impact parameter or $L = 0$) was significantly different for helium. The model of Pan and Starace is also in excellent agreement with relative measurements for hydrogen, which show a minimum at 90°.

It has been suggested that the marked difference between hydrogen and helium for scattering perpendicular to the beam direction could be the result of a combination of polarization of the target by the incident electron and correlation between the two atomic electrons in helium. It is easy to see that polarization of the hydrogen charge cloud would decrease scattering perpendicular to the beam direction and increase scattering along the forward beam direction. On the other hand, an incident electron approaching a helium atom at zero impact parameter would tend to align the two atomic electrons perpendicular to the beam direction, leading to electrons being preferentially ejected at 90°.

Neither Pan and Starace nor JM explicitly include polarization or correlation in their models, yet both models simulate the local maximum. How then, can the above simple idea be correct? First, it should be noted that correlation is included implicitly through the use of Hartree-Fock wavefunctions. Test calculations in the JM model show that if the Hartree-Fock wavefunction is replaced by an "uncorrelated" wave function, i.e., $\psi_{1s} = (8/\pi)^{1/2}\exp(-2r)$, then the maximum at 90° is greatly reduced. Thus, the correlation contained in the Hartree-Fock wavefunction significantly affects the 90° maximum. It would be very interesting to include polarization effects explicitly and/or a better treatment of exchange in the JM calculation to see if this is the cause for an underestimation of the 90° peak. Unfortunately, this is not yet feasible.

The calculation of Crothers is the dotted line in Fig. 10. Results from this calculation are only available for

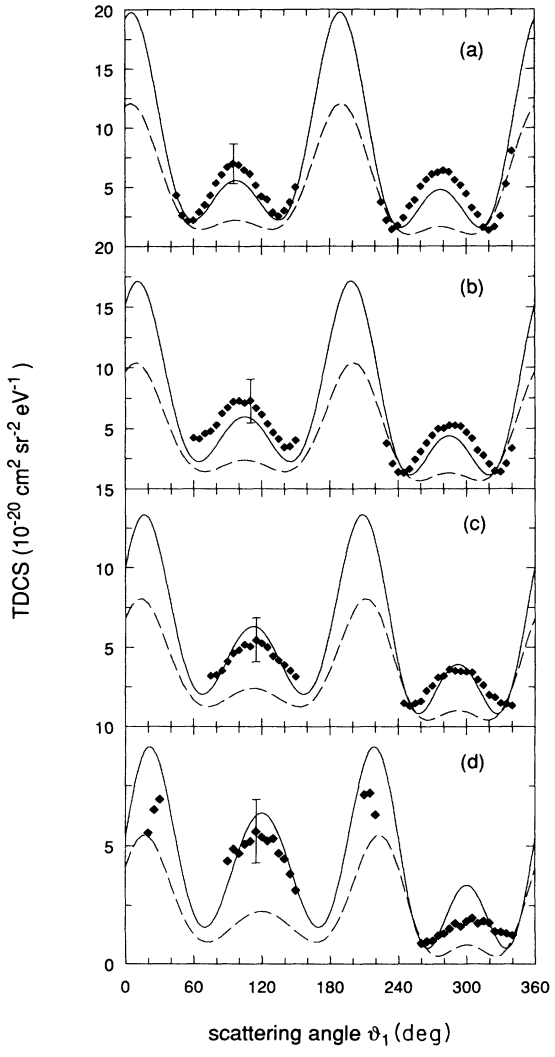

FIG. 11. The measured absolute TDCS for coplanar geometry with $\vartheta_2 = \Theta_{12} - \vartheta_1$; (a) $\Theta_{12} = 165°$; (b) 150°; (c) 135°; (d) 120°. Theory: JM solid line; JMS, dashed line.

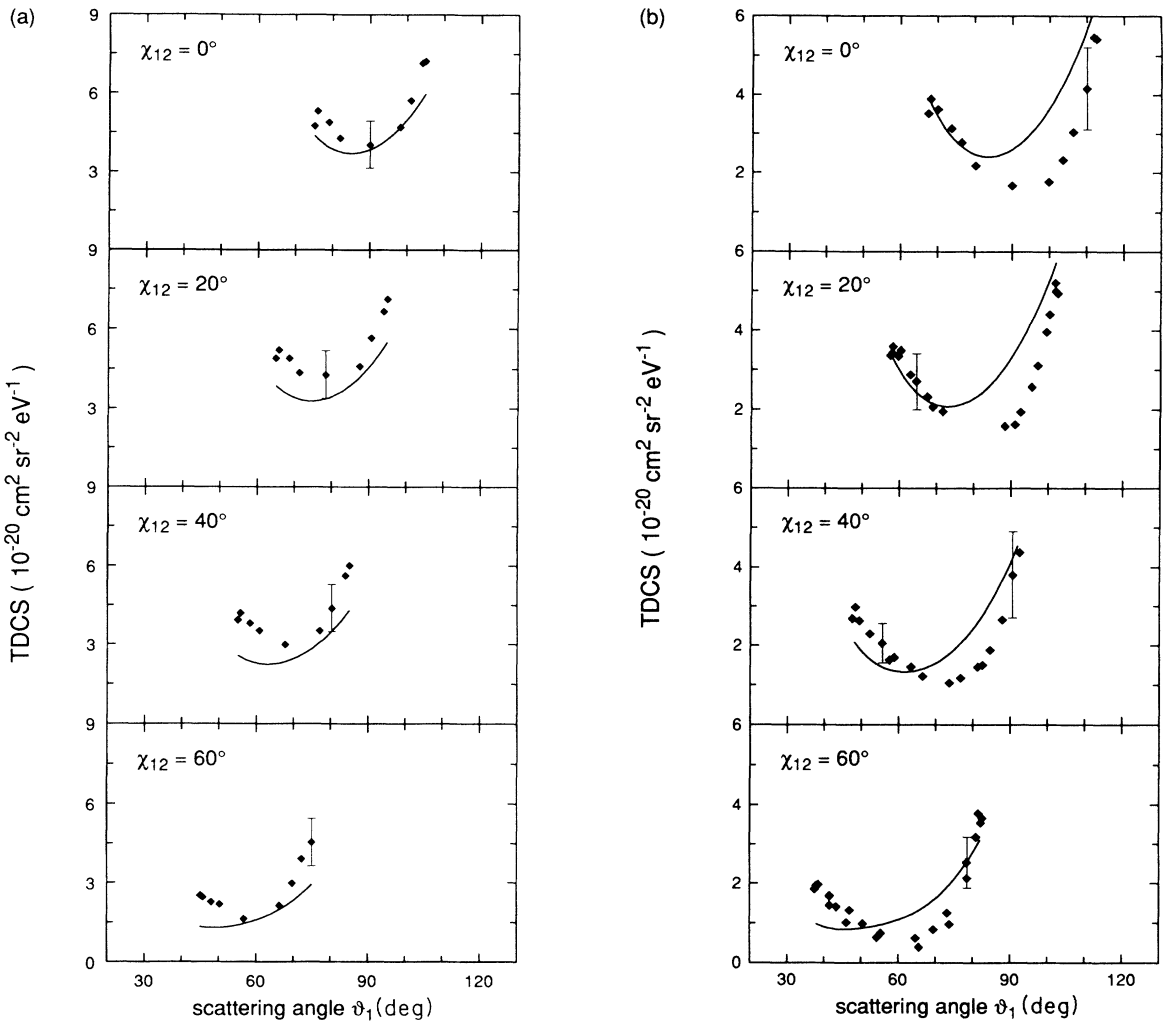

FIG. 12. (a) The measured absolute TDCS for out-of-plane kinematics with $\Theta_{12}=150°$ and $\chi_{12}=0°$, 20°, 40°, 60° (from top to bottom). Theory: JM, solid line; (b) as in (a), but $\Theta_{12}=135°$; (c) as in (a), but $\Theta_{12}=120°$; (d) as in (a), but $\Theta_{12}=105°$.

the angular range $40<\vartheta_1<140°$. It is interesting, and somewhat puzzling that the Crothers model, with its emphasis on the final state interaction (a plane wave is used for the incident electron), also achieves good agreement with the data near $\vartheta_1=90°$ since we find that it is essential to also include the short-range interactions in the initial state wave function. Thus, despite the success of Pan and Starace's calculation, the physics governing the angular distribution is still not completely understood.

Further light is shed on the reaction by examining a progression of experiments for kinematics in which the effects of the electron-electron interaction are gradually increased. Figure 11 compares JM (solid line) and JMS (dashed line) coplanar results for Θ_{12} ranging from 165° down to 120°. Recall that the only significant difference between the JMS and JM model is that the JM model includes exchange distortion. It can be seen from this figure that exchange distortion provides greatly improved agreement with experiment, both in shape and absolute magnitude. It should be noted that the best agreement between experiment and the JM model occurs here for $\Theta_{12}=135°$ whereas for Fig. 9 it was seen that the JM shape was best for Θ_{12} greater than 135°. This observation further demonstrates that effects other than the final-state interactions (Θ_{12}) are very important under different kinematical conditions.

Next, we generalize constant Θ_{12} kinematics to include out-of-plane results. The top set of figures in Figs. 12(a) through (d) show results for $\Theta_{12}=150°$, 135°, 120°, and 105°, with $\vartheta_1=\vartheta_2$. Since $\vartheta_1=\vartheta_2$ corresponds to singlet scattering, these out-of-plane results provide a detailed test for how well the singlet amplitude is modeled. From these figures we see that the strong backscattering predicted by the JM model is essentially correct although the amount of backscattering is overestimated.

The above test can be further refined. Defining the an-

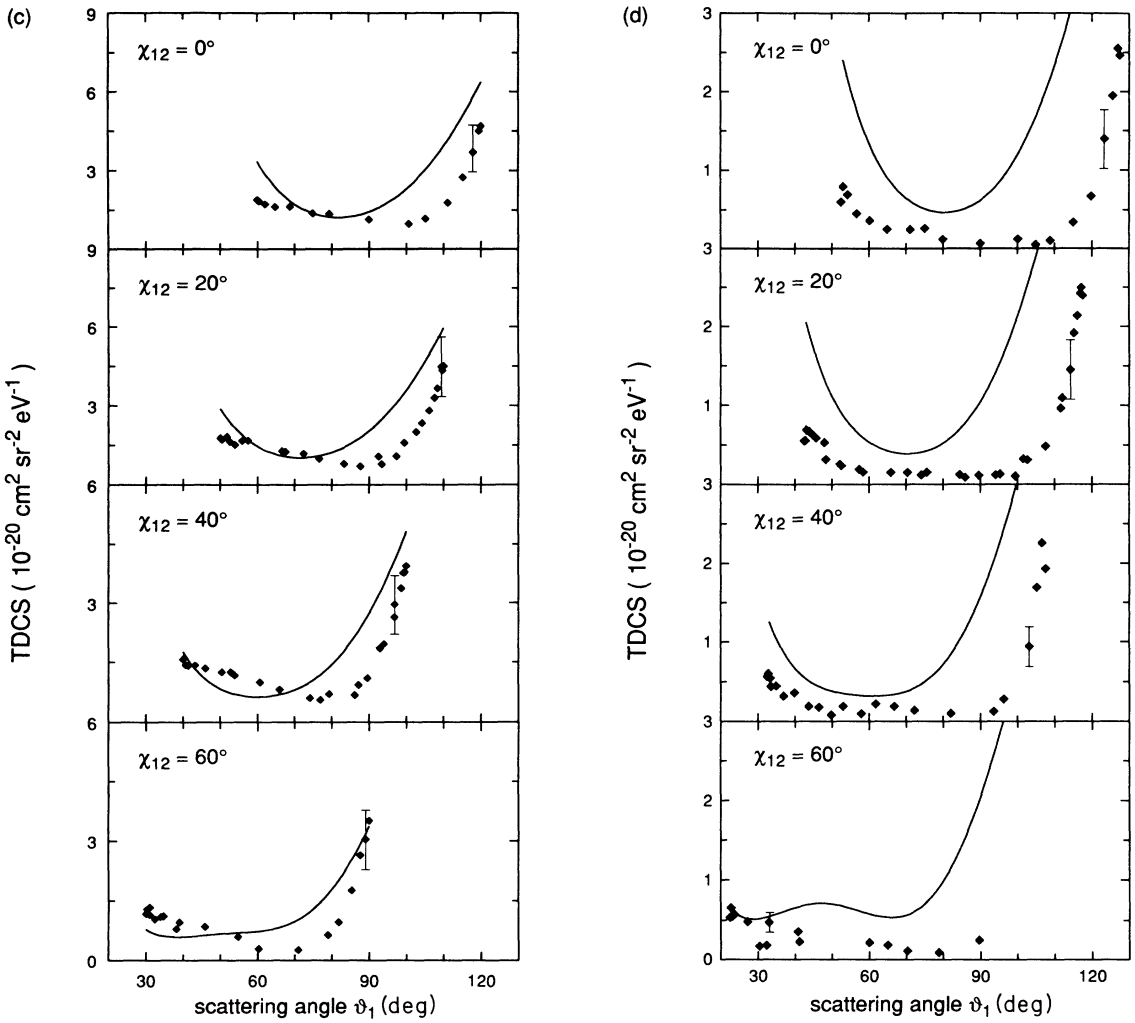

FIG. 12. (*Continued*).

gle $\chi_{12}=\vartheta_2-\vartheta_1$, the above kinematics represent scattering with Θ_{12} constant and $\chi_{12}=0°$. The choice of $\chi_{12}=0°$ suppressed triplet scattering. Other choices of χ_{12} permit progressive inclusion of the triplet components. Thus any theory that provides good agreement with the above test of the singlet components should be further tested by comparison with data for other χ_{12} values, to determine if the triplet scattering components are also well modeled. From Fig. 12 it is seen that the degree of agreement or disagreement between experiment and the JM theory is not changed, for better or for worse, by including triplet contributions.

V. CONCLUSION

We have reported theoretical and absolute experimental results for the triple-differential cross section for near-threshold ionization of helium. The out-of-plane measurements have shown that it is not possible to simply extrapolate these results from in-plane measurements. Furthermore, a partial-wave analysis of nearly 200 data points using $L=0$, 1, and 2 was not able to provide unambiguous results. This is partly due to unavoidable limitations on the range of accessible angles.

A comparison between absolute experimental results and theory provides a very sensitive test of different aspects of theoretical models near the threshold. Contributions due to distortions in the incident channel, to electron-electron repulsion in the final state, or to the singlet or triplet components of the amplitudes can all be tested. In addition, the results of Pan and Starace as well as the calculations reported here show that at these low energies it is not enough to merely antisymmetrize the approximate wave function—the possibility of exchange must be included *ab initio*.

While the JM model gives good results using simple effective charges to model the final-state electron-electron interaction, it would be highly desirable to perform distorted-wave calculations where this interaction is

treated on an equal footing with the electron-ion interaction. Work has commenced on incorporating the exact asymptotic boundary condition into the DWBA so that the use of effective charges can be avoided. Further experiments will be made on atomic hydrogen and on argon to help clarify the roles of exchange distortion and polarization.

ACKNOWLEDGMENTS

This research was supported by Sonderforschungsbereich 91 of the Deutsche Forschungsgemeinschaft and by the National Science Foundation. We thank D. S. F. Crothers, C. Pan, and A. F. Starace for providing calculations prior to publication.

[1] H. Ehrhardt, K. Jung, G. Knoth, and P. Schlemmer, Z. Phys. D **1**, 3 (1986).
[2] A. Lahmam-Bennani, J. Phys. B **24**, 2401 (1991).
[3] S. Jones, D. H. Madison, and M. K. Srivastava, J. Phys. B **25**, 1899 (1992).
[4] D. S. F. Crothers, J. Phys. B **19**, 463 (1986).
[5] C. Pan and A. F. Starace, Phys. Rev. Lett. **67**, 185 (1991).
[6] T. Rösel, J. Röder, L. Frost, K. Jung, and H. Ehrhardt (unpublished).
[7] P. Hammond, F. H. Read, S. Cvejanovic, and G. C. King, J. Phys. B **18**, L141 (1985).
[8] P. Fournier-Lagarde, J. Mazeau, and A. Huetz, J. Phys. B **17**, L591 (1984); P. Selles, A. Huetz, and J. Mazeau, *ibid.* **20**, 5195 (1987).
[9] H. Ehrhardt, K. H. Hesselbacher, K. Jung, and K. Willman, J. Phys. B **5**, 1559 (1972); E. Schubert, K. Jung, and H. Ehrhardt, *ibid.* **14**, 3267 (1981); T. Rösel, J. Röder, L. Frost, K. Jung, and H. Ehrhardt (unpublished).
[10] T. Rösel, C. Dupré, J. Röder, A. Duguet, K. Jung, A. Lahmam-Bennani, and H. Ehrhardt, J. Phys. B **24**, 3059 (1991).
[11] L. Frost, P. Freienstein, and M. Wagner, J. Phys. B **23**, L715 (1990).
[12] P. Selles, J. Mazeau, and A. Huetz, J. Phys. B **20**, 5183 (1987).
[13] P. Schlemmer, T. Rösel, K. Jung, and H. Ehrhardt, Phys. Rev. Lett. **63**, 252 (1989).
[14] S. Cvejanovic and F. H. Read, J. Phys. B **14**, 1841 (1974).
[15] T. J. Jones, S. Cvejanovic, F. H. Read, and M. B. Woolf, in *Proceedings of the Sixteenth International Conference on the Physics of Electronic and Atomic Collisions, New York, 1989,* edited by A. Dalgarno, R. S. Freund, M. S. Lubell, and T. B. Lucatorto (AIP, New York, 1990), p. 223.
[16] G. H. Wannier, Phys. Rev. **90**, 817 (1953).
[17] A. R. P. Rau, Phys. Rev. A **4**, 207 (1971).
[18] P. L. Altick and T. Rösel, J. Phys. B **21**, 2635 (1988).
[19] C. H. Greene and A. R. P. Rau, J. Phys. B **16**, 99 (1982); A. D. Stauffer, Phys. Lett. A **91**, 114 (1982).
[20] K. D. Shaw and P. L. Altick, J. Phys. B **19**, 3161 (1986).
[21] F. Pichou, A. Huetz, G. Joyez, and M. Landau, J. Phys. B **11**, 3683 (1978).
[22] K. N. Huang, Phys. Rev. A **28**, 1869 (1983).
[23] D. R. J. Carruthers and D. S. F. Crothers (unpublished).
[24] M. Brauner, J. S. Briggs, H. Klar, J. T. Broad, T. Rösel, K. Jung, and H. Ehrhardt, J. Phys. B **24**, 657 (1990).
[25] J. Botero and J. Macek, Phys. Rev. Lett. **68**, 576 (1992).
[26] X. Zhang, C. T. Whelan, and H. R. J. Walters, J. Phys. B **23**, L173 (1990).
[27] M. R. H. Rudge, Rev. Mod. Phys. **40**, 564 (1968).
[28] C. Pan and A. F. Starace, Phys. Rev. A **45**, 4588 (1992).
[29] C. J. Joachain, *Quantum Collision Theory* (North-Holland, Amsterdam, 1983), p. 449ff.
[30] C. Froese-Fisher, Comput. Phys. Commun. **4**, 107 (1972).
[31] J. B. Furness and I. E. McCarthy, J. Phys. B **6**, 2280 (1973).
[32] P. R. Bevington, *Data Reduction and Error Analysis for the Physical Sciences* (McGraw-Hill, New York, 1969), Chap. 11.
[33] C. T. Whelan, X. Zhang, and H. R. J. Walters (unpublished).

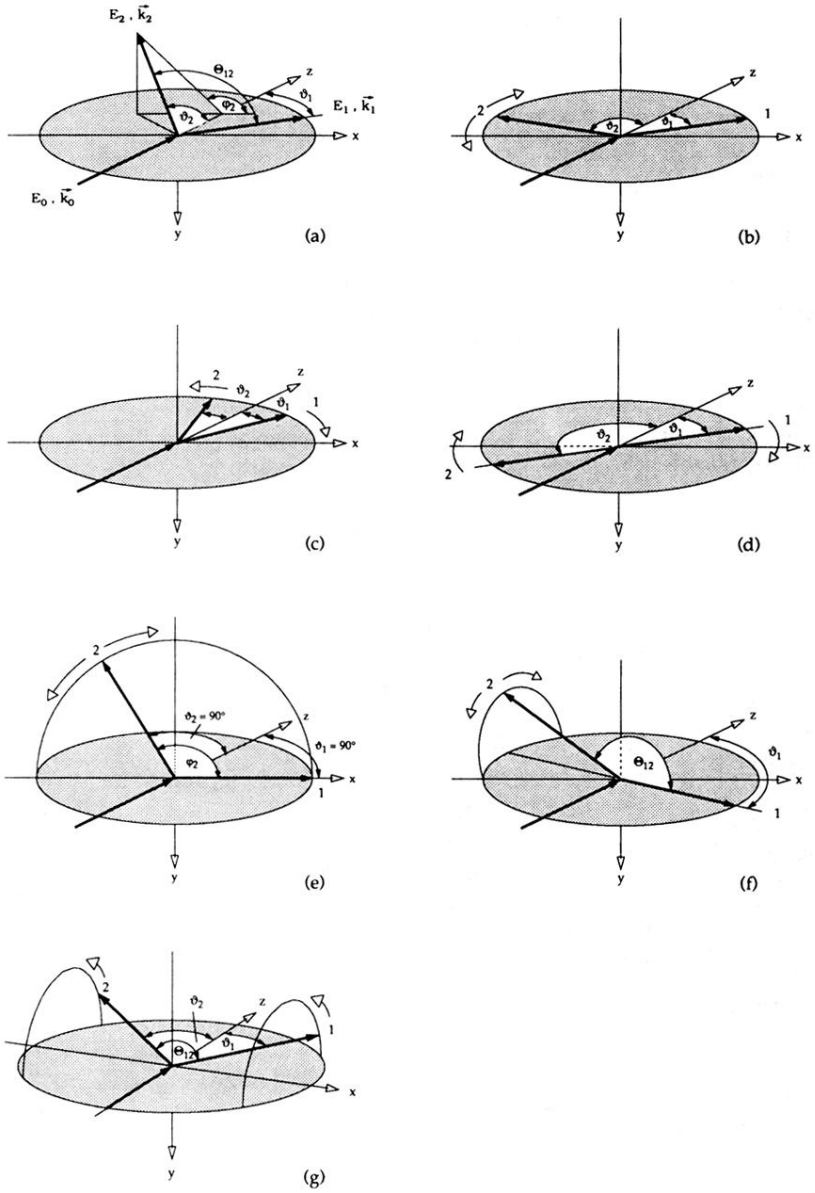

FIG. 1. Electron-impact ionization kinematics: (a) general coordinate system and experimental parameters; (b) coplanar asymmetric kinematics; (c) coplanar symmetric kinematics; (d) coplanar constant mutual angle Θ_{12}; (e) perpendicular plane kinematics; (f) noncoplanar constant mutual angle Θ_{12} for fixed ϑ_1; (g) noncoplanar constant mutual angle Θ_{12} and constant $\chi_{12}=\vartheta_2-\vartheta_1$.

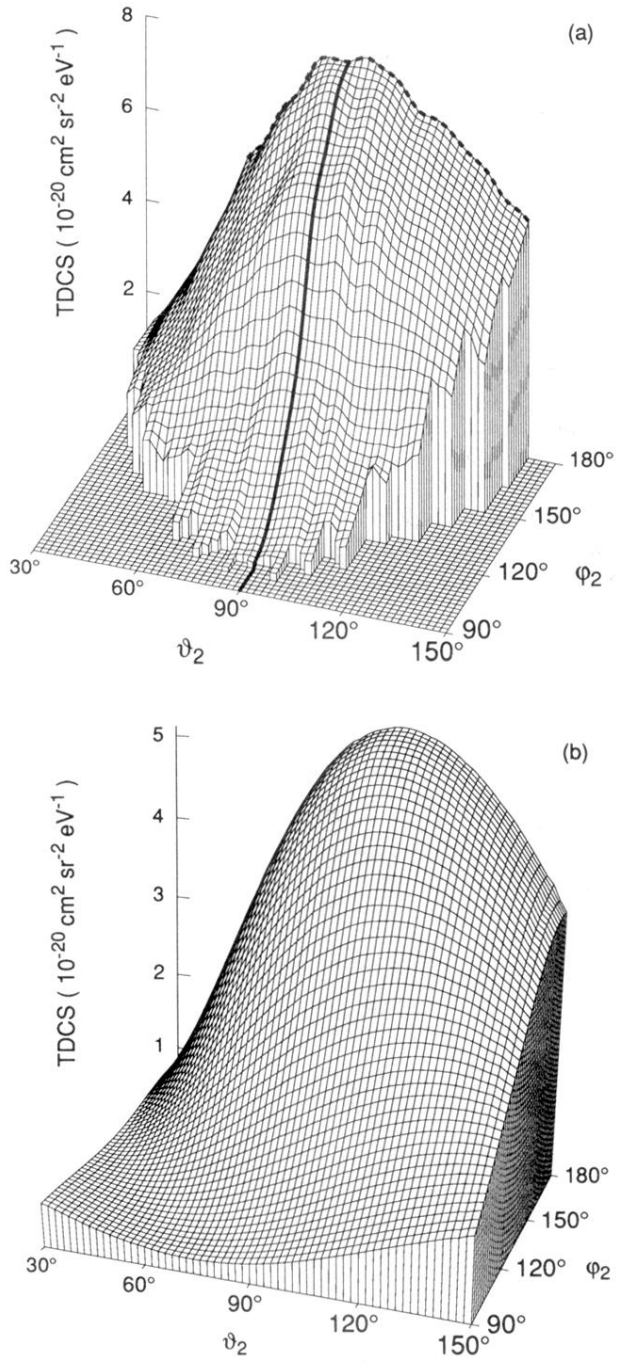

FIG. 3. (a) The measured absolute TDCS as in Fig. 2, but in rectangular coordinates where $\varphi_2 = 180°$ represents in-plane scattering; (b) the calculated cross section using the JM model corresponding to (a).

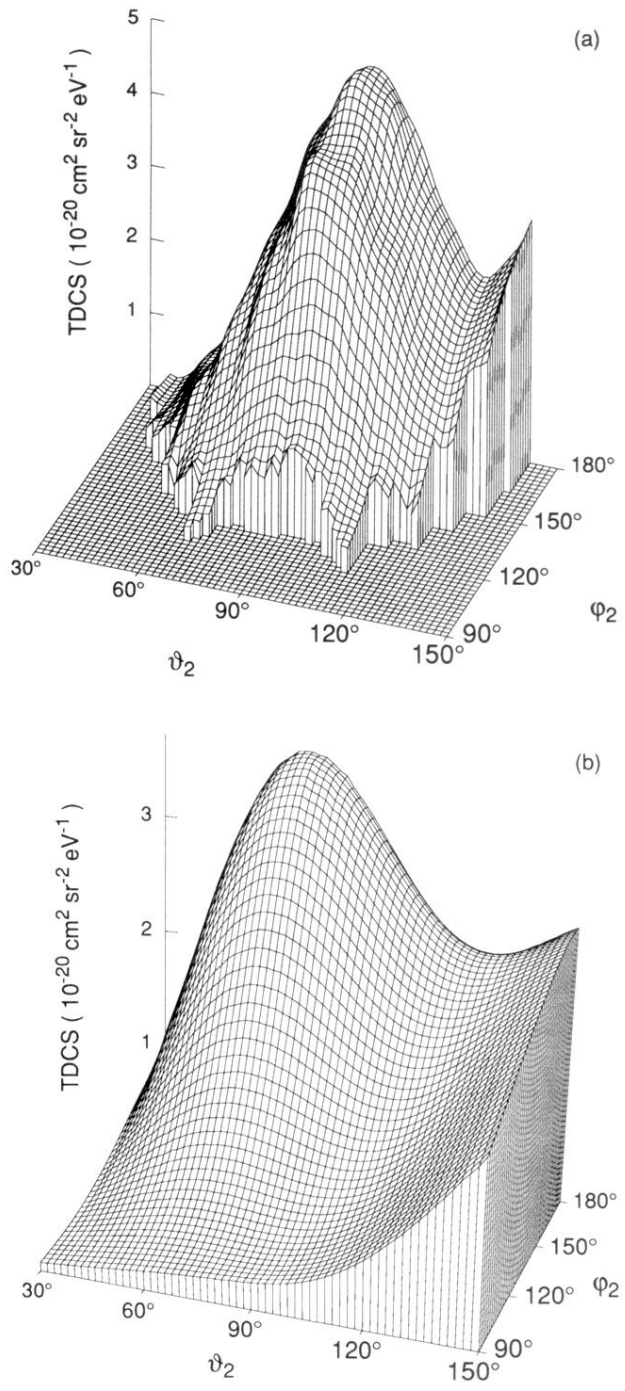

FIG. 4. (a) The measured absolute TDCS, spline-fitted as in Fig. 3, but for ϑ_1 fixed at 60°; (b) the calculated cross section using the JM model corresponding to (a).

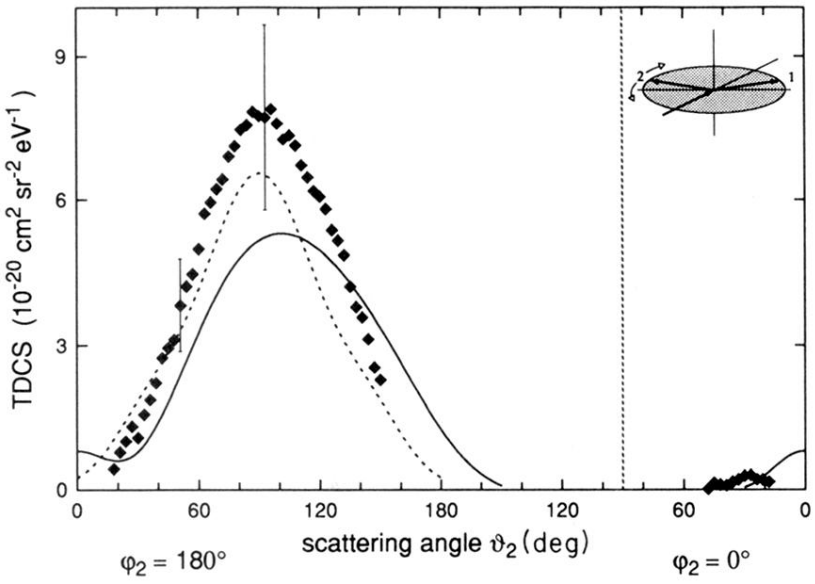

FIG. 5. The measured absolute TDCS for $\vartheta_1 = 90°$ and $\varphi_2 = 0°$ or $\varphi_2 = 180°$. The vertical dashed line indicates the position of detector 1. Detector 2 is rotated within the scattering plane. This corresponds to the measurement fitted by the dashed line in Fig. 2. In this figure, the dotted line shows the theoretical calculation of Crothers [4], the solid line the JM results.

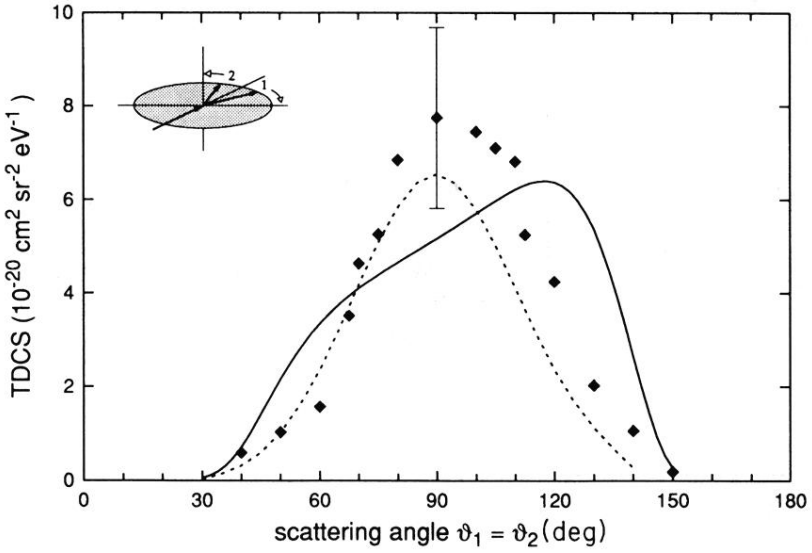

FIG. 8. The measured absolute TDCS for coplanar symmetric kinematics, $\vartheta_1 = \vartheta_2$, $\varphi_2 = 180°$. Theory: JM, solid line; Crothers, dotted line.

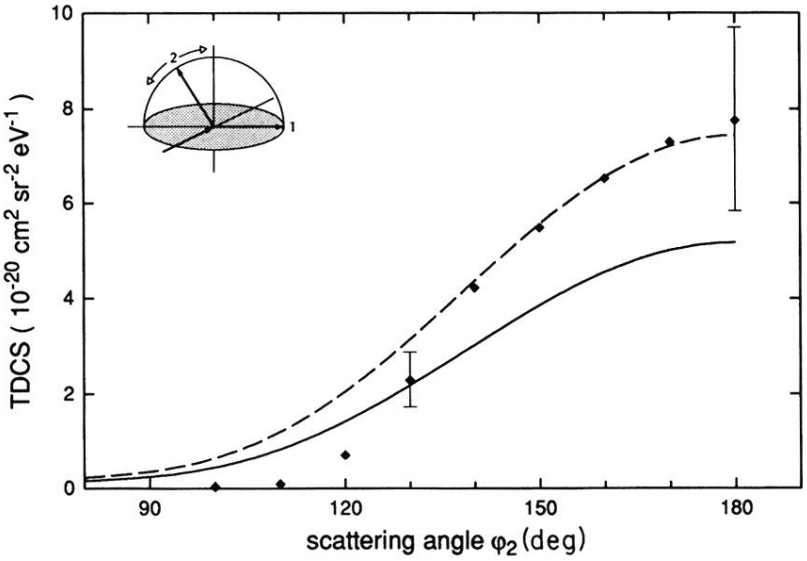

FIG. 9. The measured absolute TDCS for perpendicular plane kinematics, $\vartheta_1 = \vartheta_2 = 90°$, and φ_2 (that is, Θ_{12}) varied. The solid line is the JM result; the dashed line is the JM result, multiplied by 1.44 to allow comparison of relative shape.